Applied Catalysis B: Environmental 100 (2010) 393–402

Contents lists available at ScienceDirect

Applied Catalysis B: Environmental

journal homepage: www.elsevier.com/locate/apcatb

Effect of annealing temperature on the characteristics, sonocatalytic activity and reusability of nanotubes TiO_2 in the degradation of Rhodamine B

Yean Ling Pang, Ahmad Zuhairi Abdullah*, Subhash Bhatia

School of Chemical Engineering, Universiti Sains Malaysia, Nibong Tebal, 14300 Penang, Malaysia

ARTICLE INFO

Article history:
Received 22 April 2010
Received in revised form 27 July 2010
Accepted 18 August 2010
Available online 24 August 2010

Keywords:
Titanium dioxide nanotubes
Annealing temperature
Characteristics
Sonocatalytic activity
Reusability

ABSTRACT

Titanium dioxide nanotubes (TiO_2 NTs) were synthesized via combined sol–gel and hydrothermal method and annealed at various temperatures. The morphology and crystalline structures of the prepared TiO_2 NTs were characterized using scanning electron microscope (SEM) equipped with energy dispersive X-ray spectroscopy (EDS), transmission electron microscope (TEM), X-ray diffraction (XRD) and surface area analyzer. The sonocatalytic activity of the prepared TiO_2 NTs was evaluated based on sonocatalytic degradation of Rhodamine B in aqueous solution. Effects of annealing temperature were successfully elucidated and TiO_2 NTs annealed at 300 °C had the highest surface area and pore volume. Its sonocatalytic activity could increase by a factor of 3.7 times as compared to the conventional TiO_2 powder. Sonocatalytic activity of the annealed TiO_2 NTs decreased with increasing annealing temperature above 300 °C due to the destruction of tubular structure, a decrease in the surface area and pore volume and phase transformation from anatase to rutile. Reusability study did not reveal any significant drop in the efficiency for 4 successive cycles under investigation. The morphology, catalyst composition, specific surface area, pore size and pore volume were also investigated after each catalytic cycle.

1. Introduction

Chemical effect of ultrasound results from the phenomenon of acoustic cavitation which consists of the formation (nucleation), rapid growth (expansion) and violent collapse (implosion) of cavitation bubbles in a liquid [1]. Cavitation bubbles are generated during rarefaction cycles where negative acoustic pressure is sufficient to pull water molecules from each other to create tiny microbubbles [2]. The collapse of these cavitation bubbles could generate local high temperatures (up to 5000 K) and high pressures (above 1000 atm). Under such extreme conditions, the locally generated hot spots will be capable of sonolyzing water (H_2O) molecules to produce highly reactive species including hydroxyl (•OH), hydrogen (•H) and hydroperoxyl (•OOH) radicals [3,4]. These radicals are capable of initiating and promoting transformation reactions to mineralize organic pollutants.

The similarity between photocatalytic and sonocatalytic processes is the requirement to restrain the recombination of electron–hole pairs for enhancing the catalytic activity of semiconductor catalysts [5–7]. Sonocatalytic process occurs based on the sufficient energy obtained from acoustic cavitation which equals to or is greater than the semiconductor bandgap energy. This will lead to the excitation of electrons from the valence band and their subsequent transfer to the conduction band, leaving behind holes at the valence band [6]. The holes will then cause oxidation reactions of adsorbed organic compounds or of organic compounds that are in close proximity to the surface of the semiconductor. The major difference between photocatalytic and sonocatalytic processes is the type of energy source that leads to the formation of free radicals to initiate the oxidation reactions [4].

However, low penetrability of UV light in water medium (limited to several millimeters), high photocatalyst loading and the screening effect by the catalyst could limit the excitation of electrons and the success in actual wastewater treatment system [4,6]. The problem of spatial limitations can be eliminated when ultrasonic irradiation is used as the energy source. Moreover, the sonochemical degradation process can transform organic compounds through either oxidation with •OH radicals or high-temperature pyrolysis reactions inside cavitation bubbles. The sonochemical and pyrolytic degradation mechanisms are usually reported to be significant at high ultrasonic frequency and power. Meanwhile, non-volatile or hydrophilic organic compounds such as Rhodamine B are more difficult to be oxidized inside cavitation bubbles. Thus, it is mostly likely to be degraded by •OH radicals at the bubble surface or in the bulk solution [8–10].

Titanium dioxide (TiO_2) is the common catalyst used in photocatalytic and sonocatalytic oxidation processes to degrade organic pollutants due to its excellent physical and chemical properties

* Corresponding author. Tel.: +60 4 599 6411; fax: +60 4 594 1013.
E-mail addresses: chzuhairi@eng.usm.my, azuhairi@yahoo.com (A.Z. Abdullah).

0926-3373/$ – see front matter © 2010 Elsevier B.V. All rights reserved.
doi:10.1016/j.apcatb.2010.08.016

[4,11,12]. The advantages of TiO_2 include high catalytic activity, high chemical stability, low cost and non-toxicity. Recently, TiO_2 in the form of tubular structure has attracted the interest of numerous researchers for the potential applications in wastewater purification [13–15]. Furthermore, higher sedimentation rate of the TiO_2 NTs renders them viable to be reused as heterogeneous catalysts [16]. However, report on the use of nanotubes TiO_2 in sonocatalytic degradation of organic pollutants is hardly found in the literature. Currently, there are several techniques to synthesize TiO_2 nanotubes (TiO_2 NTs) which comprise assisted template method, electrochemical anodization, sonochemical synthesis and hydrothermal method [17]. However, the mechanism of the formation of nanotubes structure is still the subject of intense research efforts.

To date, most of the researches have been focused on the preparation and photocatalytic activity of TiO_2 NTs [13–16]. It is very rare to find research work dedicated to evaluate the influence of post-heat treatment on microstructure and surface properties of TiO_2 NTs, especially to forecast the sonocatalytic performance of TiO_2 NTs. In this study, TiO_2 NTs were prepared using alkaline hydrothermal treatment with various heat treatments and subsequently used as the sonocatalyst to degrade Rhodamine B. The effects of annealing temperature on the morphology, phase structures, crystallization, specific surface area, pore structures and sonocatalytic activity of TiO_2 NTs were investigated and discussed. The main special feature of TiO_2 NTs is its high surface-to-volume ratio as compared to that of powder form, due to its large specific surface area provided by inner and outer surfaces of the tubular structure. This could result in more surface available for the separation of electron–hole pairs to enhance the electron transfer and the interpenetration of holes transport materials due to the delocalization of charge carriers in nanotubes [18,19]. As a result, this might enhance the catalytic activity and increase the sonocatalytic degradation efficiency. Meanwhile, an attempt had also been made to study the catalytic activity and stability of TiO_2 NTs during up to 4 catalytic cycles for sonocatalytic degradation of Rhodamine B.

2. Experimental

2.1. Materials

Rhodamine B was obtained from Sigma–Aldrich as a commercially available dye. Hydrochloric acid (HCl, 37%), sodium hydroxide (NaOH, 99%), tetra-n-butyl-orthotitanate ($C_{16}H_{36}O_4Ti$ or $Ti(OBu)_4$ for synthesis, ≥98%), ethanol (CH_3CH_2OH, 96%), hydrogen peroxide solution (H_2O_2, 30%, w/w) were obtained from Merck. Potassium hydroxide (KOH, ≥98%) was purchased from System Chemical Company. All the chemical reagents were used as received. Distilled water was used throughout the study.

2.2. Preparation of TiO_2 NTs

TiO_2 powder was prepared using sol–gel method where $Ti(OBu)_4$ was first dissolved in ethanol solution at a volume ratio of 4:1 for 1 h under constant stirring. Then, a known quantity of 0.1 M HCl was added to control the pH of the solution to prevent the precipitation of TiO_2. The mixture was hydrolyzed without any further water addition at room temperature under stirring for 2 h and aged for 2 days at room temperature to obtain a dry gel. The resulting gel was washed with distilled water and dried overnight at 100 °C in an oven. After that, the gel powder was annealed at 500 °C for 3 h.

In the next preparation step, TiO_2 NTs were synthesized using hydrothermal method which was initially developed by Kasuga et al. [20] and later modified by Bavykin et al. [21]. 3.0 g of synthesized TiO_2 powder was mixed with 98 cm^3 of 10 M NaOH and 2 cm^3 of 10 M KOH solution in a Teflon vessel. The mixture was then heated at 100 °C under reflux for 48 h. The resulting white powder was thoroughly washed with distilled water to remove excess Na^+ ions. Then, the powder was repeatedly treated with 0.1 M of HCl until the washing solution reached pH 3 to promote the complete exchange of Na^+ by H^+. Then, it was washed with water before drying in an oven for 12 h at 100 °C. Finally, the dried samples were annealed at various temperatures (300–900 °C) for 2 h and were denoted as TiO_2 NTs-300, TiO_2 NTs-500, TiO_2 NTs-700, TiO_2 NTs-900 according to their respective annealing temperatures.

2.3. Sample characterization

The structure and morphology of the prepared samples were analyzed using a scanning electron microscope (SEM) equipped with energy dispersive X-ray spectroscopy (EDS), Zeiss Supra 35VP, operated at 10–15 kV. Small amounts of the powder samples were also dispersed in ethanol and the suspension was dropped onto a perforated carbon film supported on a copper grid. After drying, the droplet was observed using a transmission electron microscope (TEM). The TEM analyses were performed using a Phillips CM 12 transmission electron microscope equipped with an image analyzer and operated at 120 kV. Powder X-ray diffraction (XRD) method was used for crystal phase identification and estimation of the crystallite size. The XRD measurements were recorded using a Philips PW 3040/60 X'Pert PRO powder diffractometer, with monochromatized CuK_α radiation ($\lambda = 1.5418$ Å) and a graphite monochromator in the 2θ range of 10–80°. The particle size for the selected samples was calculated from the peak width using the Scherrer equation [4]. Detail derivation of both equations has been discussed by Spurr [22]. The weight fractions of the anatase and rutile phases of the nanotubes after being subjected to various heat treatments were estimated based on the corresponding strongest relative peak intensities using Eqs. (1) and (2) as below [4,22,23]:

$$W_A = \left[1 + 1.26\left(\frac{I_R}{I_A}\right)\right]^{-1} \quad (1)$$

$$W_B = \left[1 + 0.8\left(\frac{I_A}{I_R}\right)\right]^{-1} \quad (2)$$

where I_A and I_R are the X-ray integrated intensities of reflection of anatase and rutile, respectively. The specific surface area, pore size and pore volume measurements were determined using a surface analyzer (Micromeritics, ASAP-2020) and the results obtained were based on nitrogen adsorption–desorption data at 77.35 K.

2.4. Sonocatalytic degradation of Rhodamine B and analysis of liquid samples

Sonocatalytic degradation process of Rhodamine B was carried out in a glass reactor filled with 200 mL of aqueous dye solution at a concentration of 50 mg/L and containing 2 g/L TiO_2 NTs. The suspension was stirred for 10 min to ensure a good dispersion of the TiO_2 catalyst before ultrasonic irradiation. Ultrasonic irradiation was achieved by means of an ultrasonic bath (Elma Transsonic series TI-H5), which was operated at a frequency of 35 kHz and an effective power output of 50 W through manual adjusting. Under these mild ultrasonic conditions, degradation of organic substances due to sonolysis process is generally reported to be quite low [4,6]. After a certain period of sonocatalytic reaction, a liquid sample aliquot was withdrawn and centrifuged at 4000 rpm (Kubota 2100) to separate the catalyst. The concentration of the samples was determined using an Aquamate™ Plus UV–vis spectrophotometer (Thermo Scientific Company) to calculate the degradation of

Rhodamine B. The concentration of Rhodamine B was detected at its maximum absorbance of 554 nm. The degradation efficiency of Rhodamine B is defined as follows:

$$\text{Degradation efficiency}\,(\%) = \frac{C_0 - C_t}{C_0} \times 100\% \quad (3)$$

where C_0 is the initial concentration of Rhodamine B and C_t is the concentration of Rhodamine B at reaction time t (min). Sonocatalytic activities of the annealed TiO_2 NTs samples were evaluated by comparing the apparent reaction rate constants (k) in the batch operation. It was assumed that the sonocatalytic degradation of Rhodamine B satisfactory followed a pseudo-first-order kinetics as reported by other researchers [5,1]. The first-order kinetic reaction is expressed as $\ln(C_0/C_t) = kt$. For each sonocatalytic degradation test of Rhodamine B, three experimental runs were conducted to obtain an average value of the rate constants.

2.5. Reusability study of the TiO_2 NTs

After the sonocatalytic degradation reaction, TiO_2 NTs catalysts were collected by centrifuging the whole ultrasonic treated samples. Then, the catalysts were washed at least three times with distilled water and subsequently dried in an oven at 100 °C for 5 h. After that, the TiO_2 NTs catalyst was reused for the degradation of Rhodamine B in order to perform the next cycle of sonocatalytic degradation process. Sonocatalytic degradation process was conducted again in a glass reactor filled with 200 mL of aqueous dye solution at a concentration of 50 mg/L loaded with 2 g/L used TiO_2 NTs. The degradation efficiency of Rhodamine B within 3 h of ultrasonic irradiation was investigated for up to 4 catalytic cycles.

3. Results and discussion

3.1. SEM and TEM studies

In order to investigate the mechanical strength and thermal stability of TiO_2 NTs, the prepared samples were subjected to different annealing temperatures up to 900 °C. Figs. 1 and 2 show the morphology of TiO_2 NTs through the analysis of SEM and TEM images, respectively. Tubular morphology was clearly observed in the sample annealed at 300 °C (Figs. 1(a) and 2(a)). It was observed that the TiO_2 NTs were open-ended and the wall thickness generally varied among one another. The unequally distributed layers in the left and right side of wall shell tube indicated that the formation mechanism of nanotubes followed the helical scrolling from a single-layer nanosheet [16]. From Fig. 2(a), the average diameter of NTs was 10–15 nm with lengths ranging from several hundred nanometers to several micrometers.

A part of the tubular structure of TiO_2 NTs started to disappear when the sample was annealed at a temperature of 500 °C (Figs. 1(b) and 2(b)). Combination of shapes was recognized at the end of the nanotubes of nanoparticles TiO_2 and the diameter

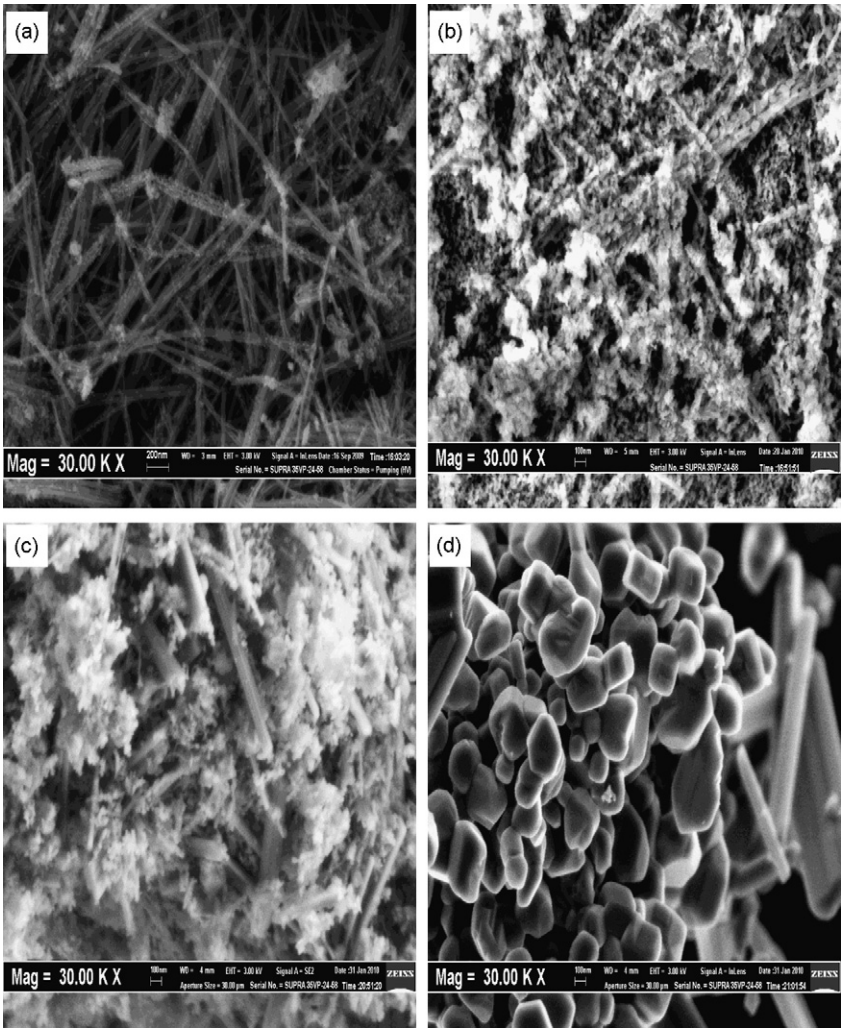

Fig. 1. SEM images of annealed TiO_2 NTs at (a) 300 °C, (b) 500 °C, (c) 700 °C and (d) 900 °C for 2 h.

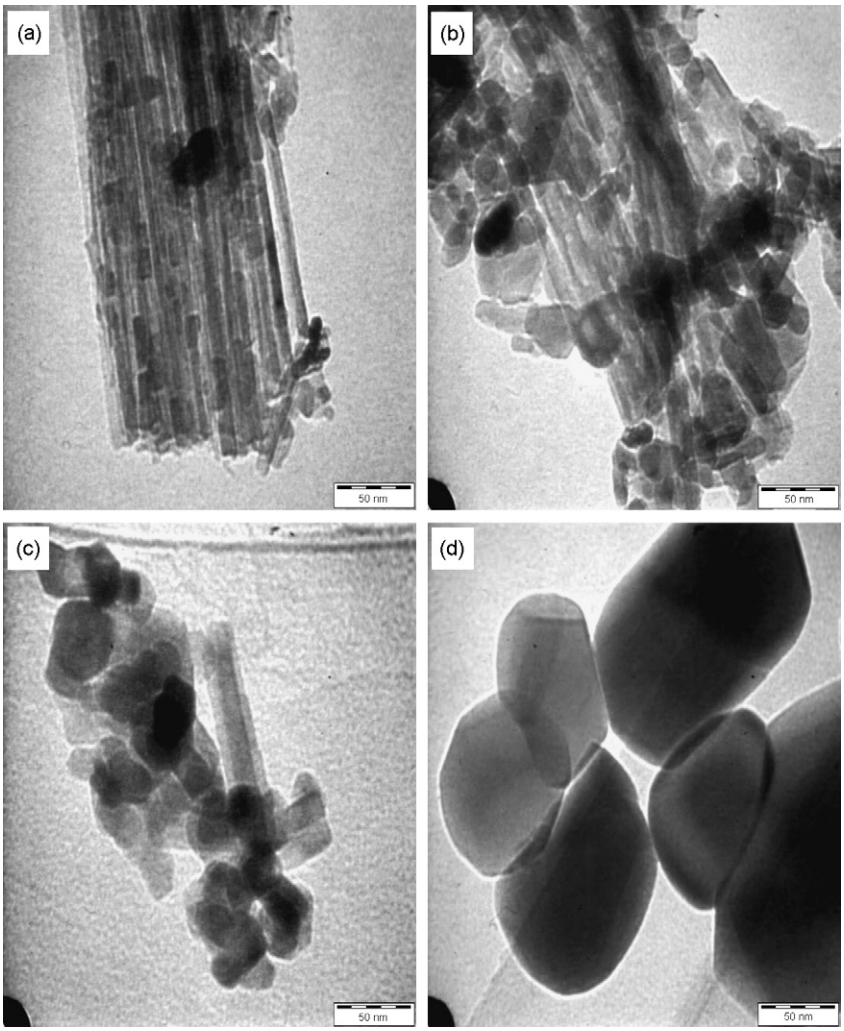

Fig. 2. TEM images of annealed TiO_2 NTs at (a) 300 °C, (b) 500 °C, (c) 700 °C and (d) 900 °C for 2 h.

of nanotubes turned wider as compared to the samples annealed at 300 °C. Zhang et al. [24] reported that the destruction of the morphology of TiO_2 NTs was mainly due to the dehydration of intralayered and interlayered OH group. When the temperature was increased to 700 °C, it could be observed that the structure changed into nanorod-shape rather than tubular structures as shown in Figs. 1(c) and 2(c). The samples became more aggregated and the TiO_2 particles were at diameters that ranged between 20 and 50 nm.

It should be noted that similar results were obtained by Inagaki et al. [13] and Yoshida et al. [25] who reported that the TiO_2 NTs prepared under hydrothermal condition could only keep their tubular morphology until up to 300 °C. However, Yu and Wang [15] found that the tubular structure of TNs prepared by electrochemical anodization was stable up to 600 °C. This study concluded that the thermal stability of tubular structure was different for every synthesis method of TiO_2 NTs. Meanwhile, Zhang et al. [24] and Qamar et al. [26] concluded that the quantity of sodium ions present in the nanotubes samples played a significant role in the stability and phase transformation of the nanotubes.

Fig. 1(d) and 2(d) show the SEM and TEM images, respectively for the sample annealed at 900 °C. It can be seen that the initial nanotubes completely disappeared and were replaced by dense aggregated rutile grains with size in the range of a few hundred nanometers. This can be attributed to the phase transformation of anatase to rutile, resulting in an obvious growth of TiO_2 crystals. Besides, small amounts of short nanorods can be observed in Fig. 1(d). Yoshida et al. [25] reported that the partially ion exchanged nanotubes (sodium ions substituted with protons) annealed at 800 °C or higher would form a mixture of sodium hexatitanates (short nanorods), anatase and rutile. However, the amount of short nanorods formed was too small and thus it was below the detection limit for XRD patterns in this study.

The composition of the TiO_2 NTs annealed at 300 °C was determined by energy dispersive X-ray spectroscopy (EDS) experiments. The presence of sodium (Na) as the minor component in TiO_2 NTs could be easily seen, because the average atomic % for 3 spots was titanium (27.21%), oxygen (68.54%) and sodium (4.25%). The result suggests that sodium ions were not completely removed by protons after washing with HCI aqueous solution and distilled water during preparation of nanotubes. Therefore, Na^+ was deemed to be partially integrated into the TiO_2 NTs structure as reported by Morgado et al. [27] and Yoshida et al. [25]. The nominal composition of the present nanotubes would be expressed as $\sim H_{1.5}$, $Na_{0.5}Ti_3O_7$ [25].

3.2. XRD patterns

Phase composition, crystallite size and crystallinity of TiO_2 are reported to have great influence on the sonocatalytic activity [28]. Therefore, crystallinity study of the samples had been conducted. Fig. 3 shows the XRD patterns of TiO_2 NTs samples annealed at temperatures between 300 and 900 °C to reveal the changes of phase structure and crystallite size after the high temperature treatment.

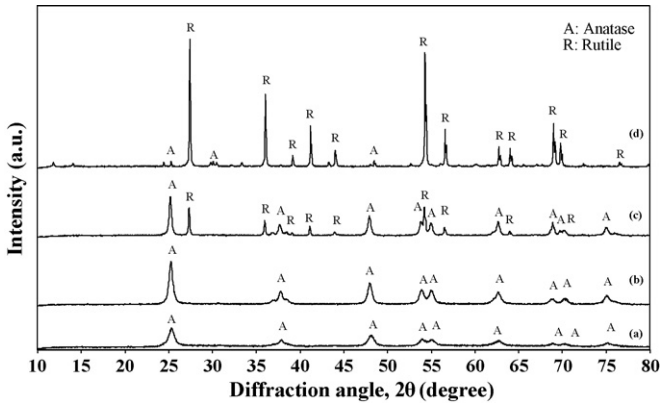

Fig. 3. XRD patterns of annealed TiO_2 NTs at (a) 300 °C, (b) 500 °C, (c) 700 °C and (d) 900 °C for 2 h.

The appearance of peaks at $2\theta = 25.38$ and 48.18 indicates the formation of anatase type TiO_2 by the heat treatment. The increase in the intensity of anatase peaks and the decrease in the width of the peaks with the increasing annealing temperature from 300 to 700 °C are indicative of the formation of TiO_2 crystallites and the improvement/growth of crystallization, respectively. Table 1 lists the calculated values of average crystalline sizes and phase composition of TiO_2 TNs samples annealed at different temperatures based on the highest peaks that appear in Fig. 3. The average crystal sizes for both anatase and rutile increased with increasing annealing temperature to indicate that higher annealing temperature would promote crystallite growth.

A rutile type TiO_2 (48.1%) was clearly observed based on a peak appearing at $2\theta = 27.58°$ in the sample that was annealed at 700 °C. This suggests that the increasing annealing temperatures would accelerate phase transformation from thermodynamically metastable anatase to the more stable and more condensed rutile phase. It should be noted that Sreekantan et al. [23] also reported that the formation of rutile phase on TiO_2 NTs using electrochemical anodization method occurred at around 700 °C. Thus, despite the difference in the methods used for nanotubes synthesis, it was proven that the annealing temperature at 700 °C or higher would induce the transformation from anatase to rutile phase of nanotubes.

In addition, transformation temperature from anatase to rutile phase of TiO_2 depends on several factors. Firstly, Tsai and Teng [29] revealed that phase transformation temperature from anatase to rutile increased with increasing synthesis temperature of nanotubes. Besides, our previous result also showed that the temperature required for phase transformation of TiO_2 powder was around 1000 °C [4] which was significantly higher than that of the currently prepared TiO_2 NTs. As the annealing temperature was increased to 900 °C, the intensity of rutile peaks significantly increased indicating that more anatase phase was transformed into rutile phase. Composition of the phases in TiO_2 was estimated according to Eqs. (1) and (2) (Table 1). The rutile composition and its crystalline size could reach up to 95.7% and 88 nm, respectively.

Table 1
XRD results of the annealed TiO_2 NTs.

Samples	Average crystal size (nm)		Phase composition (%)	
	Anatase	Rutile	Anatase	Rutile
TiO_2 NTs-300	14.9	–	100	–
TiO_2 NTs-500	24.4	–	100	–
TiO_2 NTs-700	31.4	50.5	51.9	48.1
TiO_2 NTs-900	58.4	88.0	4.3	95.7

Table 2
BET surface area, pore size and pore volume of the annealed TiO_2 NTs.

Samples	Surface area (m^2/g)	Pore size (nm)	Pore volume (cm^3/g)
TiO_2 NTs-300	150.8	8.35	0.50
TiO_2 NTs-500	61.6	18.46	0.32
TiO_2 NTs-700	32.1	22.40	0.13
TiO_2 NTs-900	4.9	7.63	0.01

3.3. BET surface area, pore size and pore volume

The BET surface area, pore size and pore volume of the different annealed TiO_2 NTs are listed in Table 2. It is clearly observed that the higher the annealing temperature, the lower the BET specific surface area and pore volume, which was in accordance with the previous observations reported by Qamar et al. [26] and Yu et al. [30]. The BET surface area was 150.8 m^2/g with an annealing at 300 °C and sharply reduced to 4.9 m^2/g after annealing at 900 °C. Firstly, this might be attributed to the increasing loss of tubular structures as shown in Figs. 1 and 2 with the increasing annealing temperature. Secondly, it could be due to the changes in the dimensions and skeletal density of nanotubes during the formation of intermediate tunnel structure as reported by Lee et al. [31]. Lastly, it might be related to the fact that the transition from anatase to rutile type TiO_2 when increasing the annealing temperatures would decrease the surface area [17].

Fig. 4 shows the nitrogen adsorption–desorption isotherms of the annealed TiO_2 NTs samples. According to IUPAC classification [32], the adsorption–desorption isotherms were of the irreversible type IV, indicating the occurrence of capillary condensation in the mesopores channel. It can be seen that TiO_2 NTs annealed at 300 °C show a type of H3 hysteresis loop of N_2 isotherms. Similar type of hysteresis loop of N_2 isotherms for TiO_2 NTs annealed at 500 °C and 700 °C was observed. The H3 loops indicated the presence of mesopores (2–50 nm) and a stronger character of disordered slit-shaped pores [27].

Meanwhile, the loops when approaching $P/P_0 \approx 1$ suggested the presence of macropores size and transformation of the pores from plate-shaped to slit-shaped pores [32]. These pores size might be attributed to the pores between nanotubes. On the other hand, Bavykin et al. [33] revealed that their nanotubes samples showed a combination of H1 and H3 type hysteresis loops with uniform pore sizes inside nanotubes. The slightly different characteristic of TiO_2 NTs might be due to the different conditions used during the

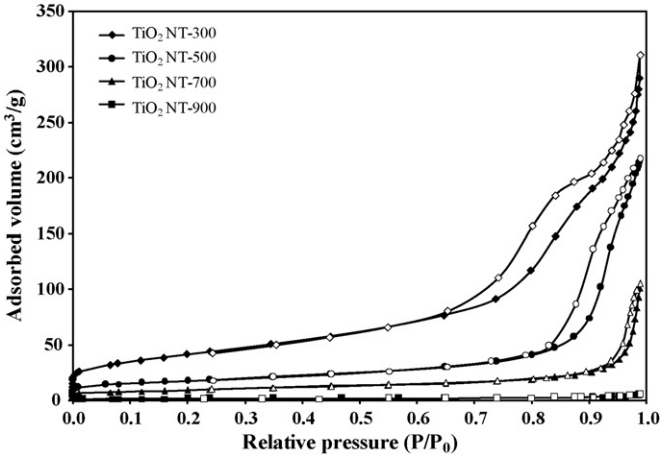

Fig. 4. Nitrogen adsorption–desorption isotherms on the surface of TiO_2 powder and NTs at different annealed temperatures (filled and open symbols indicate adsorption and desorption, respectively).

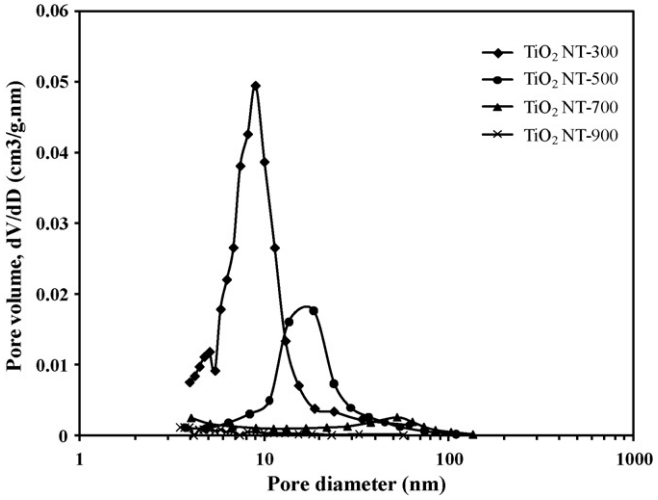

Fig. 5. Pore size distributions of TiO_2 treated at different annealed temperatures obtained from BJH desorption.

catalyst preparation. It is known that the width of the hysteresis loop is influenced by the distribution of pore sizes, and it becomes smaller with increasing annealing temperatures. For instance, no hysteresis loop could be observed when TiO_2 NTs were annealed at 900 °C.

The corresponding pore size distributions of the annealed TiO_2 NTs at various temperatures are presented in Fig. 5. It can be observed that the pore size distribution of TiO_2 NTs strongly depends on the annealing temperatures. TiO_2 NTs annealed at 300 °C showed a bimodal pore size distribution. It consists of smaller pores (≈4–6 nm) which may correspond to the pore size inside the nanotubes (inner diameter of nanotubes) while the larger pores (≈6–20 nm) reflected the aggregation of the nanotubes. The pore distributions shifted to larger pore diameter and the smaller pore disappeared when the TiO_2 NTs were annealed at 500 °C. This was attributed to the destruction of the majority of the tubular structures during the annealing. After annealing at 700 °C or 900 °C, the pore size distribution peak could not be clearly observed and it was due to the crystals agglomeration and the presence of rutile-phase TiO_2. The average pore size of the annealed TiO_2 NTs increased with annealing temperature until 700 °C as shown in Table 2. This might be due to the collapse of tubular structures as the inner pore size experienced greater stress as compared to the larger pores formed by the aggregation of nanotubes as reported by Lee et al. [31].

3.4. Sonocatalytic activity of TiO_2 NTs after annealing at various temperatures

Sonocatalytic activity of TiO_2 NTs was evaluated through the degradation of a basic dye i.e. Rhodamine B in an aqueous solution under ultrasonic irradiation for up to 3 h. The removal of Rhodamine B in the presence of TiO_2 powder and TiO_2 NTs-300 °C was confirmed by a drop in the absorbance peak within visible wavelength as shown in Fig. 6(a) and (b), respectively. Minero et al. [8] reported that when the alteration of the shape of the spectrum was not significant, it indicated that there was no colored degradation intermediates produced. Thus, in this case, the spectral interference along the reaction time was negligible. Similar results were obtained by Wang et al. [34] on the sonocatalytic degradation of Rhodamine B in the presence of ZnO catalyst after 120 min. However, specific trend in UV wavelengths (200–400 nm) was not observed in this study as the small (colorless) degradation products such as ultimate gaseous and volatile products would simply

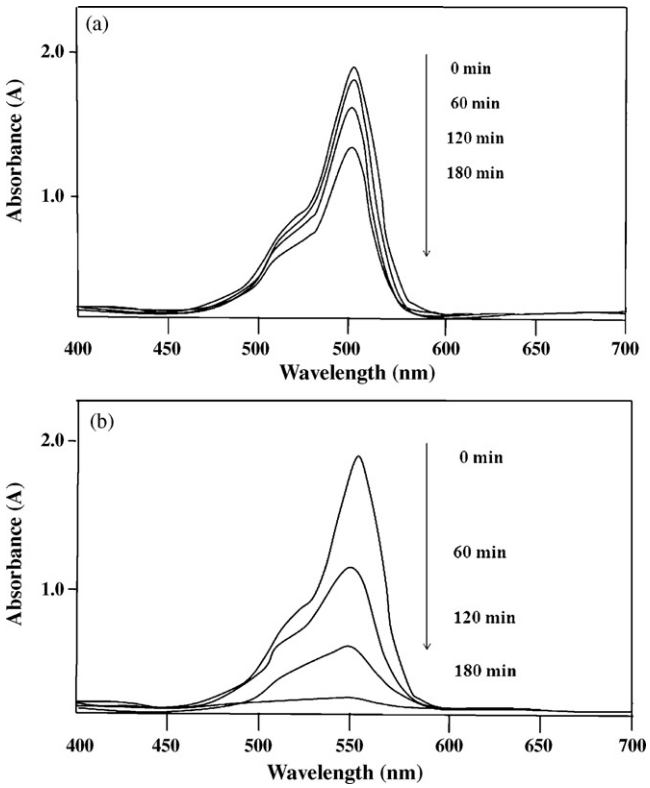

Fig. 6. Changes in the absorbance during the sonocatalytic degradation of Rhodamine B in the presence of (a) TiO_2 powder and (b) TiO_2 NTs-300.

escape from the reaction mixture. Fig. 7 shows the sonocatalytic degradation of Rhodamine B in the presence of various annealed TiO_2 NTs. The sonolysis of Rhodamine B without catalyst was only 14% after 180 min. The increase in the degradation rate in the presence of catalyst was due to the presence of solid particles in a liquid which increased the nucleation sites for cavity formation. Once undergoing electron shifts from the valence band to the conduction band, TiO_2 NTs itself could also act as a catalyst to promote water dissociation reactions. The combined effects led to the generation of more free radicals in the aqueous system. In order to compare the sonocatalytic activity among the annealed TiO_2 NTs, sonocatalytic degradation of Rhodamine B with the presence of TiO_2 powder was also performed and the corresponding k value was 2.26×10^{-3} min^{-1} (or 2.93×10^{-9} g/min cm^2 when divided by the specific surface area).

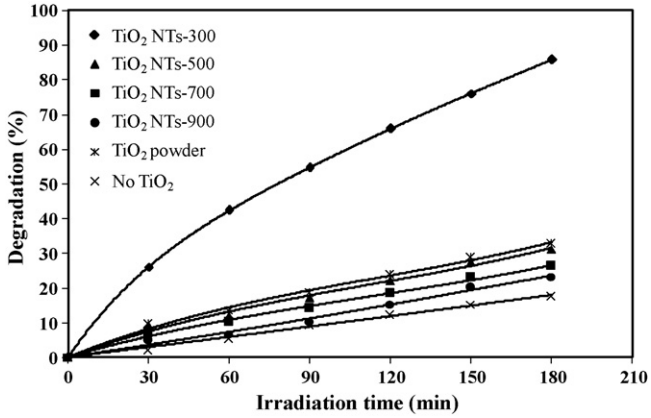

Fig. 7. Degradation efficiency of Rhodamine B versus irradiation time for various annealed TiO_2 NTs.

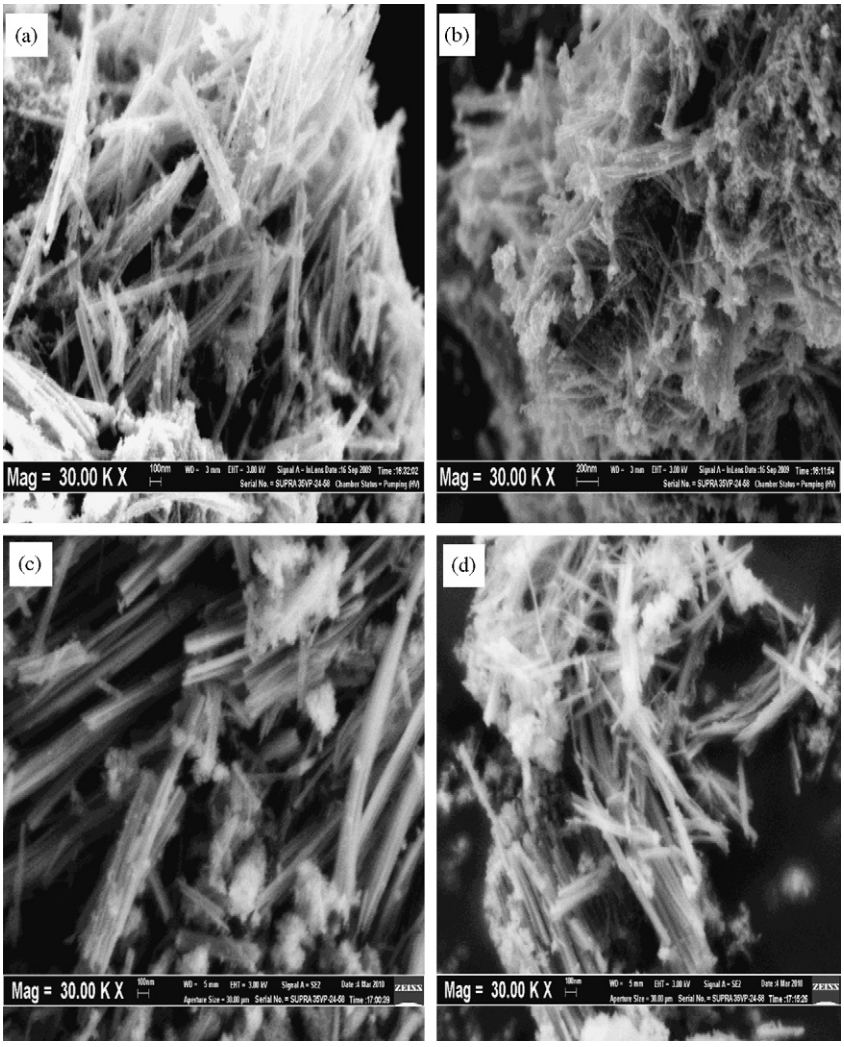

Fig. 8. SEM images of TiO_2 NTs-300 after ultrasonic irradiation for (a) 3 h, (b) 6 h, (c) 9 h and (d) 12 h.

Experimental results showed that increasing annealing temperature of TiO_2 NTs resulted in a decrease in the efficiency of sonocatalytic degradation of Rhodamine B. It should be noted that the k value for sonocatalytic activity of the TiO_2 NTs-300 °C was 8.49×10^{-3} min^{-1} (5.63×10^{-9} g/min cm^2) and exceeded that of the TiO_2 powder sample by a factor of 3.8 (or 1.9 for the surface area-specific k). Among the characteristics of TiO_2 NTs-300 °C, it had the largest specific surface area and pore volume as compared to the samples that were annealed at higher temperatures. It was often reported that larger specific surface area would allow more Rhodamine B reactants to adsorb onto the surface of the catalyst, while higher pore volume would result in more rapid diffusion of various compounds during the sonocatalytic reaction [30]. When k value is taken to be independent of the specific area of the catalyst, the main factor to increase the degradation rate constant was associated with the increased delocalization of charge carriers in nanotubes, where the separated electrons and holes were free to move throughout the length of the tubes. This could reduce the recombination probability [19]. Then, the electrons would be captured by the surface-adsorbed O_2 molecules to yield $^{\bullet}O_2^-$ and $^{\bullet}$OOH radical ions, while the holes would oxidize the organic dyes adsorbed on the surface of TiO_2 particles, directly or through the generation of $^{\bullet}$OH radicals upon oxidation of H_2O molecules [6]. Rhodamine B would then undergo degradation with this pool of reactive transients.

Recently, Lee et al. [31] reported improved results of photocatalytic degradation of the basic dye BV10 in the presence of TiO_2 NTs annealed at 300 °C as compared with P25. Meanwhile, Yu et al. [30] and Sreekantan et al. [23] revealed that TiO_2 NTs annealed at 400–500 °C possessed higher photocatalytic activity as compared to TiO_2 NTs annealed at 300 °C. This could be mainly due to the experimental conditions such as surface morphology of tubular structure retained on a porous structure that was similar to that of the sample annealed at 300 °C. In our case, tubular structure was hardly observed when the TiO_2 NT was annealed at 500 °C. However, the negative effects caused by the decrease in surface area and pore volume were compensated by the positive effect provided by an improvement in the crystallization of anatase phase. The k value for TiO_2 NTs-500 °C was 2.11×10^{-3} min^{-1} (3.43×10^{-9} g/min cm^2) which was smaller than that of TiO_2 NTs-300 °C and TiO_2 powder. Further increase in the annealing temperature of TiO_2 NTs would lead to a gradual decrement of the sonocatalytic activity. At 900 °C, the k value significantly decreased to 1.42×10^{-3} min^{-1} (2.90×10^{-8} g/min cm^2). It should be noted that significant increase in the surface area-specific k value was observed in this study as rutile phase is generally reported to retard the recombination of electron–hole on the surface of the semiconductor catalyst [4,6]. However, the positive effect was completely offset by significant reduction in the surface area available for the reaction. This observation indicated that the phase transformation from

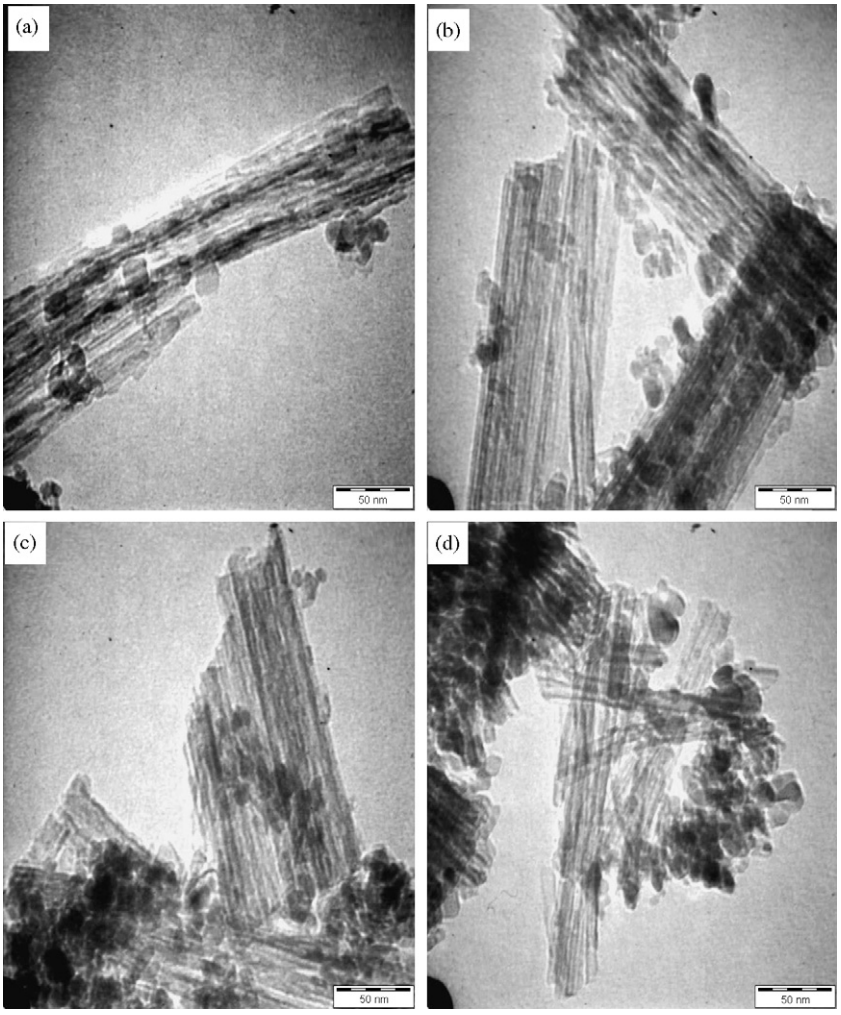

Fig. 9. TEM images of TiO_2 NTs-300 after ultrasonic irradiation for (a) 3 h, (b) 6 h, (c) 9 h and (d) 12 h.

anatase to rutile phase, sintering and growth of TiO_2 crystallites which are responsible for the decrease in surface area and pore volume could have different effects on the reaction rate. In this study, the highest apparent activity was demonstrated by TiO_2 NTs-300. Thus, only this catalyst was used to investigate the reusability of the catalyst for sonocatalytic degradation of Rhodamine B.

3.5. Catalytic stability of the used TiO_2 NTs

According to the key principles of green chemistry, effective catalysis and the catalyst recovery are vital to feasibility of the process to decrease contaminants from wastewater [35]. In fact, the phenomenon of catalyst deactivation is of utmost concern for chemical investigation. If the stability of a catalyst is poor, it will be difficult to apply it in industry. In addition, the detailed effects of ultrasonic irradiation on the surface morphology and properties of TiO_2 NTs were rarely reported in earlier publications. Thus, there is a need to investigate the recovery, reusability, catalytic activity and characteristics of the TiO_2 NTs for their possible continuous use as heterogeneous sonocatalysts to treat wastewater.

The morphology of the TiO_2 NTs after undergoing ultrasonic irradiation to degrade Rhodamine B in aqueous solution was examined by using SEM and TEM. Figs. 8 and 9 show the SEM and TEM images at the same magnification for the used and fresh catalysts. In order to distinguish the main structural differences between fresh and reused catalysts, samples that underwent 12 h of ultrasonic irradiation (Figs. 8(d) and 9(d)) were compared to the freshly annealed TiO_2 NTs at 300 °C (Figs. 1(a) and 2(a)). It was found that the distance between tubular structures became smaller and shorter nanotubes were observed as compared to the fresh sample. Consequently, a more compact structure of TiO_2 NTs could be observed (Fig. 8(c) and (d)). Similar results were obtained by Bavykin et al. [33] after 2 h of ultrasonic treatment. Meanwhile, tubular structures partially disappeared where long nanotubes were broken down into shorter nanotubes.

To support the argument that ultrasonic irradiation only caused a slight change to the tubular structures, the elemental composition of the used catalysts were investigated using EDS analysis (data not shown). There was no significant change in the Ti and Na contents which implied that the catalysts had good structure stability and no significant leaching of elements occurred. Fig. 10 shows that the XRD patterns of the used TiO_2 NTs were quite similar to the fresh catalyst. It was found that there was no obvious difference between the used and fresh TiO_2 NTs to indicate that ultrasonic irradiation hardly affected the crystallites of catalysts.

Table 3 presents the BET surface area, pore size and pore volume of the used TiO_2 NTs in each successive cycle. It was clearly observed that there was a slight decrease in the specific surface area during the ultrasonic irradiation. Yu et al. [36] reported that the implosive collapse of bubbles caused transformation of the surface morphology and enhanced the crystallization of the catalyst. The decreased

Table 3
BET surface area, pore size, pore volume and apparent reaction rate constant (k) of the fresh and reused TiO_2 NTs-300.

Samples	Surface area (m^2/g)	Pore size (nm)	Pore volume (cm^3/g)	k ($\times 10^{-3}$ min^{-1})
TiO_2 NTs-300	150.8	8.35	0.50	8.49
TiO_2 NTs-300-1	149.7	8.14	0.43	8.05
TiO_2 NTs-300-2	147.7	7.42	0.43	7.75
TiO_2 NTs-300-3	146.0	7.39	0.42	7.27
TiO_2 NTs-300-4	140.8	6.79	0.39	6.73

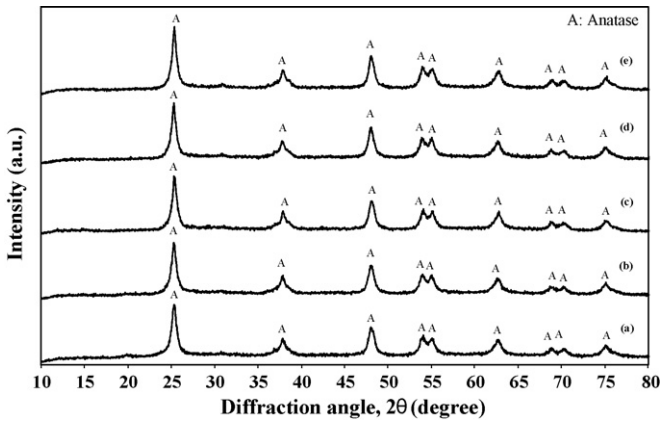

Fig. 10. XRD patterns of TiO_2 NTs-300 after ultrasonic irradiation for (a) 0 h, (b) 3 h, (c) 6 h, (d) 9 h and (e) 12 h.

in surface area was mainly attributed to the effect of the destruction of short nanotubes to form non-tubular structures or nanoparticles. Meanwhile, the destruction of long nanotubes to form shorter nanotubes resulted in the increase in surface area. Thus the proportions of these two effects could decide the net effect on the specific surface area. In this case, the negative contribution negated the positive effect of increasing surface area. However, a slight decrease in surface area did not significantly affect the degradation efficiency of Rhodamine B.

The corresponding pore size distributions of the used TiO_2 NTs in each catalytic cycle are shown in Fig. 11. The figure reveals that the pore volume inside the nanotubes was not significantly affected by ultrasonic irradiation to suggest the stability of the catalyst structure. However, distribution of pore volumes in the nanotubes was reduced after 12 h of ultrasonic irradiation. The reduction of pore size and pore volume with the ultrasonic irradiation might relate to the destruction of nanotubes. These results were in good agreement with the compact structure of TiO_2 NTs as observed in SEM and TEM images.

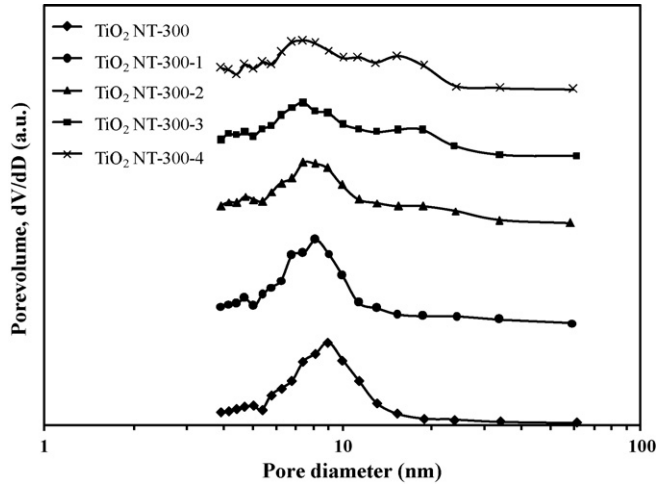

Fig. 11. Pore size distributions for the fresh and reused TiO_2 NTs-300 obtained from BJH desorption.

3.6. Sonocatalytic activity of the used TiO_2 NTs

The reusability of TiO_2 NTs was investigated for up to 4 cycles of use as shown in Fig. 12 and the corresponding apparent rate constants are presented in Table 3. The degradation efficiency of Rhodamine B in the presence of TiO_2 NTs after the second cycle was approximately 83% which was quite close to the result for the first cycle with 86% of the degradation efficiency. After the fourth cycle, the degradation efficiency was at 75% and the estimated reduction for each catalytic cycle was within 5%. It should be highlighted that our previous results showed that reused TiO_2 powder gave a dramatic decrease in Congo Red dye removal efficiency by about 10% after the second cycle [4]. Thus, TiO_2 NTs showed better activity retention under ultrasonic treatment as compared to powder TiO_2. Prado and Costa [35] reported the ability of TiO_2 NTs to be reused in photo-degradation reactions as they maintained 80% of dye degradation after 10 catalytic cycles. They revealed that the recovery of TiO_2 anatase was difficult and the re-application of these catalysts was not as effective as compared to TiO_2 NTs.

When cavitation occurs near a solid surface, high-speed jets of liquid could lead to the formation of microjets of solvent ($100\ ms^{-1}$) to hit the surface of the catalyst [37]. This would produce asymmetric shock waves and would result in continuous cleaning/renewing of the surface of the catalyst. In other words, sonication could accelerate oxidation via clearing the intermediate products or final products away from the surface of the catalyst and provide clean and available surface for subsequent reactions. Subsequently, the mass transport rates of the consequent reactions: adsorption–oxidation–desorption reactions of the Rhodamine B from the bulk solution to the surface of the nanotubes would be enhanced.

Besides, ultrasound could cause solid particle partial rupture with a consequent decrease in particle size and an increase in surface area available for the reaction to occur [37]. In our case,

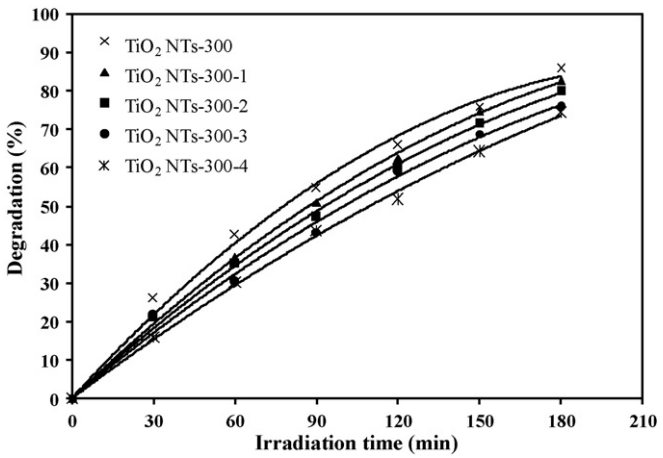

Fig. 12. Degradation efficiency of Rhodamine B versus irradiation time for the fresh and reused TiO_2 NTs-300 for 3 h.

sonication permitted the destruction of long nanotubes and formation of relatively shorter ones, resulting in larger surface area of nanotubes for oxidation reactions to occur. As a result, more reactant surface area was readily formed for the formation of nucleation sites near the surface of catalyst, thereby, promoting further sonocatalytic degradation of Rhodamine B on the surface of nanotubes. Hence, TiO_2 NTs showed excellent reuse potential with only a slight decrease in the catalytic activity.

Recently, it was reported that the sonocatalytic degradation mechanism was related to the heterocatalytic surface reaction steps of sonication reactions in water vapor and the reactions used in photocatalysis [5–7,38]. The theory of 'hot spot' is the most highly favored explanation on the sonocatalytic degradation of organic compounds [3,6,7,37]. The extreme localized conditions will produce different reactive radicals as explained earlier. Moreover, the sonoluminescence could result in the formation of the light flash of average photon energy of 6 eV [6,37,38]. This can lead to separation of electron–hole pair in the TiO_2, where they are responsible either to degrade organic compounds directly or indirectly through triggering a series of reactions leading to the formation of $^{\bullet}OH$ radicals.

4. Conclusions

The crystallites phase, surface morphology, specific surface area, pore structure and sonocatalytic activity of TiO_2 NTs were strongly influenced by the annealing temperature. This study reveals that the surface morphology of TiO_2 NTs is stable at an annealing temperature of 300 °C and the catalyst showed the highest sonocatalytic activity to degrade Rhodamine B in aqueous solution. This could be attributed to the fact that it had the largest specific area and pore volume. The presence of residual sodium ion was confirmed, and Na^+ was found to be integrated into the TiO_2 NTs structure. Ultrasonic irradiation caused slight changes in surface morphology and gradually decreased the specific surface area, pore size and pore volume until the fourth catalytic cycle. These effects might be related to the powerful microjets produced during collapsing bubbles near a solid surface, which could be responsible for pitting and erosion of the surface of catalyst. TiO_2 NTs successfully retained their high catalytic activity after the fourth catalytic cycle, implying a huge potential as stable heterogeneous catalysts in sonocatalytic degradation process.

Acknowledgements

Financial supports provided by Universiti Sains Malaysia in the form of a Research University (RU) Grant, a Post Graduate Research Grant Scheme and a Fellowship are gratefully acknowledged.

References

[1] R. Vinu, G. Madras, Environ. Sci. Technol. 43 (2009) 473–479.
[2] M.A. Behnajady, N. Modirshahla, M. Shokri, B. Vahid, Ultrason. Sonochem. 15 (2008) 1009–1014.
[3] Y.G. Adewuyi, Environ. Sci. Technol. 39 (2005) 8557–8570.
[4] A.Z. Abdullah, P.Y. Ling, J. Hazard. Mater. 173 (2010) 159–167.
[5] J. Wang, W. Sun, Z. Zhang, X. Zhang, R. Li, T. Ma, P. Zhang, Y. Li, J. Mol. Catal. A: Chem. 272 (2007) 84–90.
[6] J. Wang, W. Sun, Z. Zhang, Z. Xing, R. Xu, R. Li, Y. Li, X. Zhang, Ultrason. Sonochem. 15 (2008) 301–307.
[7] J. Wang, Z. Jiang, L. Zhang, P. Kang, Y. Xie, Y. Lv, R. Xu, X. Zhang, Ultrason. Sonochem. 16 (2009) 225–231.
[8] C. Minero, P. Pellizzari, V. Maurino, E. Pelizzetti, D. Vione, Appl. Catal. B: Environ. 77 (2008) 308–316.
[9] C. Minero, M. Lucchiari, D. Vione, V. Maurino, Environ. Sci. Technol. 39 (2005) 8936–8942.
[10] Y. Lu, L.K. Weavers, Environ. Sci. Technol. 36 (2) (2002) 232–237.
[11] X. Yang, C. Cao, L. Erickson, L. Hohn, K.R. Maghirang, K. Klabunde, Appl. Catal. B: Environ. 91 (2009) 657–662.
[12] J. Yu, Q. Xiang, M. Zhou, Appl. Catal. B: Environ. 90 (2009) 595–602.
[13] M. Inagaki, N. Kondo, R. Nonaka, E. Ito, M. Toyoda, K. Sogabe, T. Tsumura, J. Hazard. Mater. 161 (2009) 1514–1521.
[14] Y.S. Sohn, Y.R. Smith, M. Misra, V. (Ravi) Subramanian, Appl. Catal. B: Environ. 84 (2008) 372–378.
[15] J. Yu, B. Wang, Appl. Catal. B: Environ. 94 (2010) 295–302.
[16] L. Deng, S. Wang, D. Liu, B. Zhu, W. Huang, S. Wu, S. Zhang, Catal. Lett. 129 (2009) 513–518.
[17] X. Chen, S.S. Mao, Chem. Rev. 107 (2007) 2891–2959.
[18] R. Menzel, A.M. Peiro, J.R. Durrant, M.S.P. Shaffer, Chem. Mater. 18 (2006) 6059–6068.
[19] T. Tachikawa, S. Tojo, M. Fujitsuka, T. Sekino, T. Majima, J. Phys. Chem. B 110 (2006) 14055–14059.
[20] T. Kasuga, M. Hiramatsu, A. Hoson, T. Sekino, K. Niihara, Langmuir 14 (1998) 3160–3163.
[21] D.V. Bavykin, B.A. Cressey, M.E. Light, F.C. Walsh, Nanotechnology 19 (2008), art. no. 275604.
[22] R.A. Spurr, Anal. Chem. 29 (1957) 760–762.
[23] S. Sreekantan, R. Hazan, Z. Lockman, Thin Solid Films 518 (2009) 16–21.
[24] M. Zhang, Z. Jin, J. Zhang, X. Guo, J. Yang, W. Li, X. Wang, Z. Zhang, J. Mol. Catal. A: Chem. 217 (2004) 203–210.
[25] R. Yoshida, Y. Suzuki, S. Yoshikawa, Mater. Chem. Phys. 91 (2005) 409–416.
[26] M. Qamar, C.R. Yoon, H.J. Oh, D.H. Kim, J.H. Jho, K.S. Lee, W.J. Lee, H.G. Lee, S.J. Kim, Nanotechnology 17 (2006) 5922–5929.
[27] J.E. Morgado, M.A.S. de Abreu, G.T. Mour, B.A. Marinkovic, P.M. Jardim, A.S. Araujo, Chem. Mater. 19 (2007) 665–676.
[28] J. Wang, T. Ma, Z. Zhang, X. Zhang, Y. Jiang, W. Sun, R. Li, P. Zhang, Ultrason. Sonochem. 14 (2007) 575–582.
[29] C.-C. Tsai, H. Teng, Chem. Mater. 16 (2004) 4352–4358.
[30] J. Yu, H. Yu, B. Cheng, C. Trapalis, J. Molecul. Catal. A: Chem. 249 (2006) 135–142.
[31] C.-K. Lee, M.-D. Lyu, S.-S. Liu, H.-C. Chen, J. Taiwan Inst. Chem. Eng. 40 (2009) 463–470.
[32] M. Kruk, M. Jaroniec, Chem. Mater. 13 (2001) 3169–3183.
[33] D.V. Bavykin, V.N. Parmon, A.A. Lapkin, F.C. Walsh, J. Mater. Chem. 14 (2004) 3370–3377.
[34] J. Wang, Z. Jiang, Z. Zhang, Y. Xie, X. Wang, Z. Xing, R. Xu, X. Zhang, Ultrason. Sonochem. 15 (2008) 768–774.
[35] A.G.S. Prado, L.L. Costa, J. Hazard. Mater. 169 (2009) 297–301.
[36] J. Yu, M. Zhou, B. Cheng, H. Yu, X. Zhao, J. Mol. Catal. A: Chem. 227 (2005) 75–80.
[37] L.H. Thompson, L.K. Doraiswamy, Ind. Eng. Chem. Res. 38 (1999) 1215–1249.
[38] M.H. Priya, G. Madras, Ind. Eng. Chem. Res. 45 (2006) 913–921.